JOURNAL OF MATERIALS SCIENCE 33 (1998) 2047–2052

High-temperature mechanical properties of hot-pressed TiN with fine grain size

R. YAMAMOTO, S. MURAKAMI, K. MARUYAMA
Department of Materials Science, Graduate School of Engineering, Tohoku University, Sendai 980-8579, Japan
E-mail: maruyama @ material. tohoku.ac.jp

Mechanical properties of fine-grained TiN were studied by compression tests at temperatures ranging from 1073–1823 K and strain rates from 2×10^{-5} to 5×10^{-3} s^{-1}. The temperature dependence of maximum (fracture or peak) stress of TiN reveals three regions with different activation energy and strain-rate sensitivity. At lower temperatures, brittle fracture takes place without plastic deformation. Fracture stress is independent of temperature, and greater than 1 Gpa. In the intermediate temperature region, specimens fracture in a quasi-brittle manner after a few per cent plastic deformation. Fracture stress decreases above 1300 K (in the intermediate temperature region), due to the deformation-assisted fracture. TiN becomes fully ductile at further higher temperatures, at which five independent slip systems are available. This ductile to brittle transition characteristic of TiN is similar to MgO (ionic) but different from TiC (covalent), though all three materials take the same NaCl type of lattice structure. In the high-temperature region, the activation energy for plastic deformation is close to that for diffusion of nitrogen in TiN. Strain-rate sensitivity in this region is typical of superplasticity, suggesting the possibility of superplastic forming.

1. Introduction

Titanium nitride, TiN, is extensively used as hard coatings on machining tools owing to its excellent wear resistance. TiN has a high melting temperature (3200 K), relatively low specific gravity (5.4), and high resistance to corrosion and oxidation [1]. These attractive physical and chemical properties suggest potentialities of TiN as a high-temperature material. Mechanical properties of hot-pressed TiN have been studied at elevated temperatures with Vickers microhardness [2]. However, limited information is available on fundamental mechanical properties of TiN. This paper reports mechanical properties of TiN at temperatures ranging from 1073 K ($0.33T_m$. T_m is the melting temperature) to 1823 K ($0.57T_m$).

Several ceramic materials, for example MgO, TiN and TiC, take the same NaCl type of lattice structure. These ceramics, however, exhibit different types of ductile to brittle transition, because their active slip systems change with the difference in electronegativity between their constituent elements [3, 4]. The difference in electronegativity is 2.3 in MgO (ionic), 1.4 in TiN, and 0.9 in TiC (covalent). The ductile to brittle transition behaviour of TiC and MgO is schematically represented in Fig. 1 according to the literature [3]. The active slip system in TiC is $\{1\,1\,1\}\langle 1\,1\,0\rangle$ [5], and becomes operative above a critical temperature (1200 K [4] or 900 K [18]). This slip has five independent slip systems necessary for plastic deformation of polycrystals. Ductile to brittle transition, therefore, is completed within a narrow temperature range close to the critical temperature [6, 7]. In the case of MgO, on the other hand, the primary slip is $\{1\,1\,0\}\langle 1\,1\,0\rangle$, providing two independent slip systems only [3, 4]. The primary slip is active above 300 K [4]. The secondary $\{0\,0\,1\}\langle 1\,1\,0\rangle$ slip [3,4], providing the additional three independent slip systems, is available above 2000 K [4]. Polycrystalline MgO, therefore, is brittle below 300 K, and becomes fully ductile above 2000 K [8]. Quasi-brittle fracture assisted by the primary slip occurs over a wide range of temperatures from 300–2000 K because of the lack of the five independent slip systems. The difference in electronegativity of TiN is in between the two materials. Another objective of this study was to examine which type of ductile to brittle transition occurs in TiN.

2. Experimental procedure

The starting material used was ultra-fine-grained TiN powder, 30 nm diameter. The powder was hot pressed (HP) or hot pressed and then hot isostatically pressed (HIP) to discs 50 mm diameter and 5 mm thick. Sintering conditions, grain size and density of each material are listed in Table I. The four materials are designated HP0, HIP1, etc., according to the sintering processes. In order to avoid amorphous phases along the grain boundaries, the powder was compacted without any additive (HP1) or with ethyl alcohol (all others). Amorphous phases were not observed as shown in Fig. 2, even in the alcohol-added material. Chemical compositions of the materials were

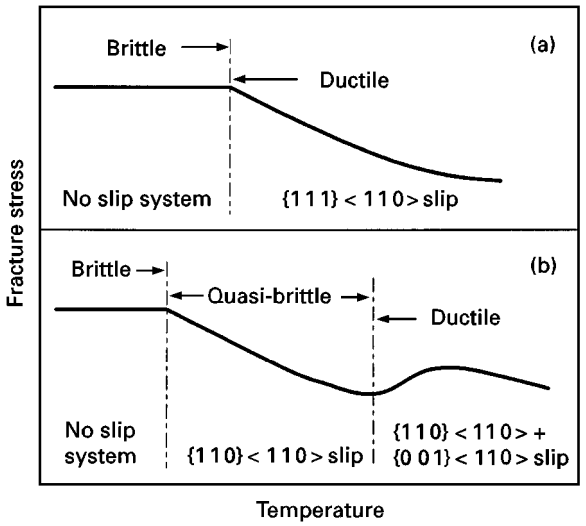

Figure 1 Temperature dependence of fracture stress and ductile to brittle transition behaviour expected in (a) TiC and (b) MgO.

TABLE I Sintering conditions, grain size, d, and density of materials studied. T, sintering temperature; t, sintering time; P, sintering pressure

Specimen	Hot pressing	HIP	d (μm)	Density
HP0	$T = 1873$ K $t = 3.6$ ks $P = 16$ MPa	No	0.3	97.8%
HP1	$T = 1873$ k $t = 3.6$ ks $P = 20$ MPa	No	1.1	96.5%
HIP1	$T = 1873$ K $t = 3.6$ ks $P = 16$ MPa	$T = 1873$ K $t = 3.6$ ks $P = 200$ MPa	1.4	~100%
HIP3	$T = 2073$ K $t = 3.6$ ks $P = 16$ MPa	$T = 2073$ K $t = 3.6$ ks $P = 200$ MPa	3.5	97.5%

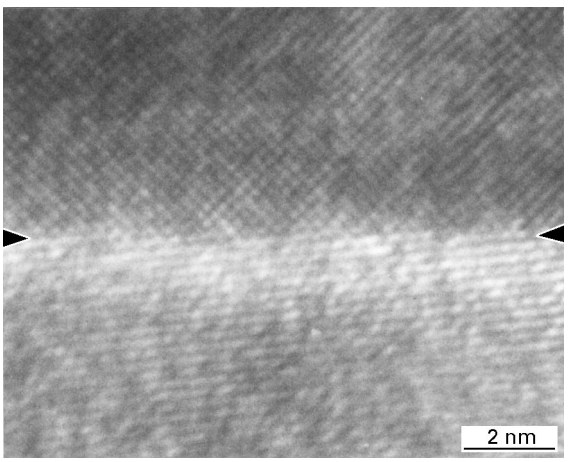

Figure 2 Lattice image of HP0. The grain boundary is indicated by arrows.

estimated from their lattice constants, based on a correlation between lattice constant and nitrogen concentration reported on TiN [9]. Their compositions are in the range of $TiN_{0.90}$ to $TiN_{0.97}$. Oxygen and carbon contents in HIP1 were measured by energy dispersive spectroscopy. The oxygen content was about 1 at %, but no carbon peak was detected. Compression specimens were cut from the sintered discs, polished with SiC, and then with diamond paste. Their final size was approximately 3 mm × 3 mm in cross-section and 4.5 mm high.

Compression tests were carried out in a vacuum (2×10^{-3} Pa) or in a nitrogen gas atmosphere at temperatures from 1073–1823 K and initial strain rates from $2 \times 10^{-5}\,s^{-1}$ to $5 \times 10^{-3}\,s^{-1}$ using an Instron testing machine. The different atmospheres did not affect mechanical properties of TiN. Specimens were indirectly heated by a graphite susceptor placed in an induction furnace. Temperature was measured by a thermocouple and kept within ± 2 K. Specimens were held at the testing temperature for 14.4 Ks prior to compression tests. BN power was used as a lubricant between the specimen and the SiC compression rods. After compression tests, specimens were cooled at 7.5 K s^{-1}, and then subjected to transmission electron microscopy (TEM). Thin foils for TEM observation were made by argon ion-milling. Microstructure was studied using a Hitachi H-800 microscope operating at 200 kV.

3. Results and discussion

3.1. Effects of temperature on mechanical properties

True stress, σ, versus true plastic strain, ε, curves of HIP1 are shown in Fig. 3. The specimens were deformed at an initial strain rate, $\dot{\varepsilon}$, of $1 \times 10^{-4}\,s^{-1}$. The flow stress decreases and the fracture strain increases with increasing temperature. Flow stress, σ, at high temperature is expressed by

$$\sigma = \left(\frac{\dot{\varepsilon}}{\dot{\varepsilon}_0}\right)^m d^{mp} \exp\left(\frac{mQ}{RT}\right) \quad (1)$$

where $\dot{\varepsilon}$ is the strain rate, $\dot{\varepsilon}_0$ a constant, m the strain-rate sensitivity, d the grain size, p the grain-size expo-

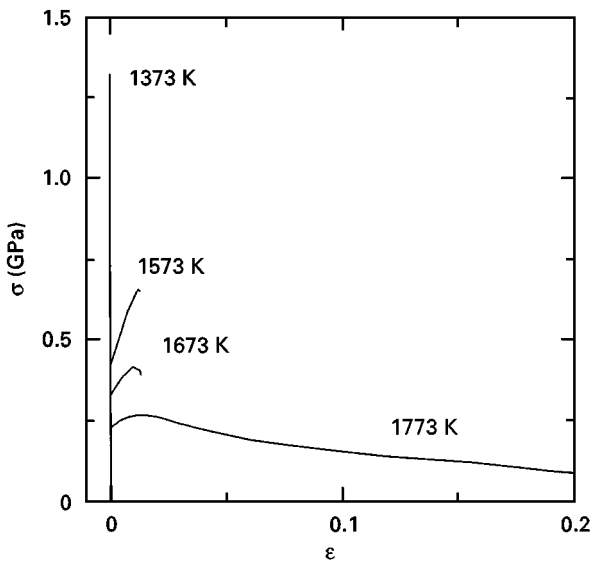

Figure 3 Representative true stress, σ, versus true plastic strain, ε, curves of HIP1 at $\dot{\varepsilon} = 1 \times 10^{-4}\,s^{-1}$.

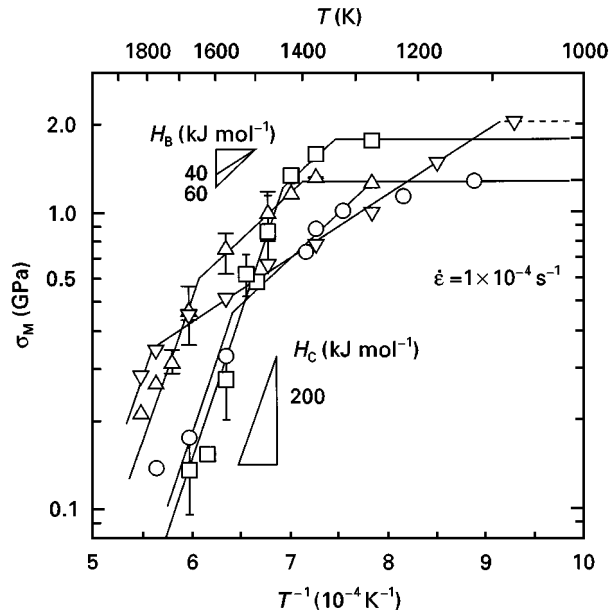

Figure 4 Maximum stress σ_M, as a function of reciprocal temperature. $H = mQ$. (□) HP0, (○) HP1, (△) HIP1, (▽) HIP3.

nent, Q the activation energy, R the universal gas constant, and T the absolute temperature. Maximum stresses, σ_M, of the four materials are plotted in Fig. 4 as a function of reciprocal temperature. The slope of $\log\sigma_M$ versus $1/T$ gives the value of mQ in Equation 1. The temperature dependence of σ_M is divided into three regions with different values of mQ. The three regions are referred to as A (low temperature), B (intermediate temperature) and C (high temperature). σ_M corresponds to fracture stress in regions A and B, and to the peak stress on a stress–strain curve in region C. The fracture stress is independent of temperature in region A, and σ_M decreases in regions B and C. The value of mQ greater in region C (200 kJ mol^{-1}) than in region B (40–60 kJ mol^{-1}). Although the boundaries between regions A and B shift among the materials, they are located around 1300 K, except for HIP3. The values of mQ in each region are similar among the four materials.

3.2. Characteristics of each region

In region A, brittle fracture takes place without any appreciable amount of plastic deformation, like the stress-strain curve at 1373 K in Fig. 3. This region corresponds to the brittle fracture regime shown in Fig. 1. Crack extension starts from pre-existing flaws, and fracture stress is determined by flaw size, which is usually related to grain size. As seen in Fig. 4, the fracture stress of TiN tends to increase with decreasing grain size. HIP3 with the largest grain size, however, gives the highest fracture stress in region A. Some other microstructural features must be taken into consideration to understand fully the fracture in this region. It is to be noted that the fracture stress of TiN is greater than 1 GPa, even at 1300 K.

At intermediate temperatures (region B), the maximum stress, σ_M, decreases with increasing temperature. This region corresponds either to the ductile regime of TiC or to the quasi-brittle regime of MgO shown in Fig. 1. Representative stress–strain curves in this region are given in Fig. 3 (1573 and 1673 K). The boundary between regions B and C does not exactly coincide with the change in the shape of stress–strain curve. 1673 K is close to the boundary, and this temperature is in region B in terms of the shape of stress–strain curve. These stress–strain curves clearly indicate quasi-brittle fracture after a few per cent plastic deformation. It follows from this fact that the MgO type of ductile to brittle transition occurs in TiN.

Grain size and porosity affect fracture stress in region B. The fracture stress is high in HP0 (small grain size) and HIP1 (low porosity), but low in HP1 (medium grain size and high porosity) and HIP3 (large grain size).

At higher temperatures, TiN reveals high ductility and remarkable strain softening, like the curve at 1773 K in Fig. 3. Region C corresponds to the ductile fracture regime of Fig. 1b. Microstructural features affecting mechanical properties in this region will be discussed in Section 3.6.

3.3. Effects of strain rate

True stress versus true plastic strain curves of HP0 deformed at 1573 K are shown in Fig. 5. The flow stress decreases with decreasing strain rate. Maximum stresses, σ_M, are plotted against strain rate, $\dot{\varepsilon}$, in Fig. 6. The logσ–log$\dot{\varepsilon}$ relations are divided into two regions with the different strain-rate sensitivity, m. As seen in Fig. 4, 1573 K is in region C at $\dot{\varepsilon} = 1 \times 10^{-4}\,s^{-1}$. The stress–strain curve at this strain rate is typical of region C (see Fig. 5). The value of m in this region is 0.58 and typical of superplasticity. This result suggests a possibility of superplastic forming of TiN.

At the higher strain rates, the stress–strain curves in Fig. 5 change to the one typical of region B; the small fracture strain. This high strain-rate region corresponds to region B, and the value of m decreases to 0.05.

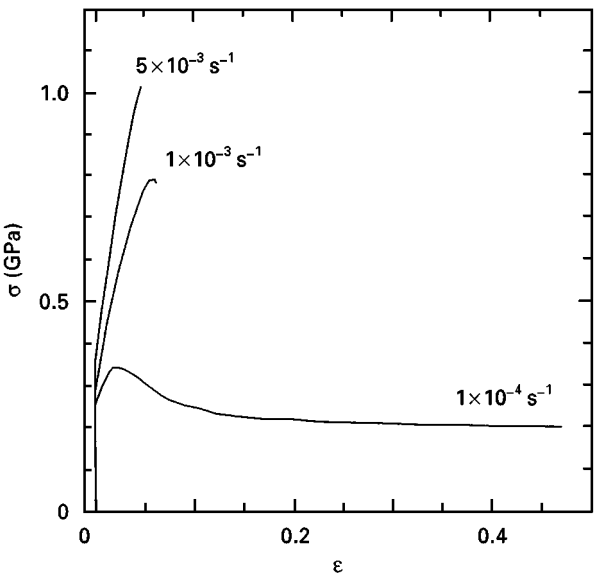

Figure 5 Change of stress, σ, versus strain, ε, curve with strain rate, ε, in HP0 at 1573 K.

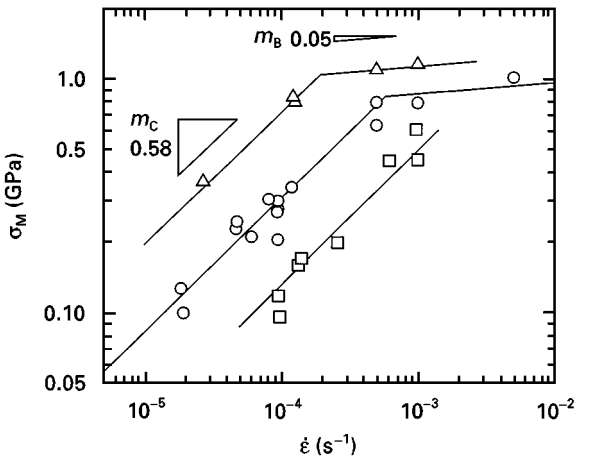

Figure 6 Maximum stress, σ_M, as a function of strain rate, $\dot{\varepsilon}$, in HP0. (□) 1673 K, (○) 1573 K, (△) 1473K.

3.4. Slip system

TiN takes a NaCl-type lattice structure. The Burgers vector of active dislocations in this type of lattice structure is known to be 1/2 ⟨1 1 0⟩ [3, 4]. Fig. 7 shows transmission electron micrographs of HIP1 deformed at $\dot{\varepsilon} = 1 \times 10^{-4} s^{-1}$ and 1823 K (region C). A number of dislocations are seen within the grain. They bow out in a direction, suggesting that they were moving during the compression test. These dislocations are visible with the diffraction condition $\boldsymbol{g} = \bar{1}\,\bar{1}\,1$, but out of contrast with $\boldsymbol{g} = \bar{2}\,0\,0$ and $\boldsymbol{g} = 1\,1\,1$. This result indicates that the Burgers vector of the dislocation is 1/2 [0 1 $\bar{1}$]. The same is true in region B. These findings confirm that ordinary 1/2⟨1 1 0⟩ is the Burgers vector of dislocations active in TiN.

As mentioned in Section 1, ductile to brittle transition is completed within a narrow range of temperature, when the active slip system is {1 1 1}⟨1 1 0⟩like TiC [6, 7]. When the primary slip is {1 1 0}⟨1 1 0⟩ like MgO, on the other hand, polycrystals reveal quasi-brittle fracture over a wide range of temperature. A similar result has been reported for UO_2 which takes a CaF_2type of lattice structure [10]. The primary slip in UO_2 is {0 0 1}⟨1 1 0⟩, providing three independent slip systems [4]. The slip is active above 1000 K [4]. The secondary {1 1 0}⟨1 1 0⟩ slip providing the additional two independent slip systems is available above 1500 K [4]. Polycrystalline UO_2, therefore, shows quasi-brittle fracture between 1000 and 1500 K.

As discussed in Section 3.2, TiN shows the quasi-brittle regime similar to MgO and UO_2. Although it was not easy to determine active slip planes in the TiN specimens because of their small grain size, dislocations do seem to be present on several slip planes other than {1 1 1}. This evidence suggests that the primary slip system of TiN is not TiC-type {1 1 1}⟨1 1 0⟩ but MgO-type {1 1 0}⟨1 1 0⟩.

3.5. Transition from quasi-brittle region B to ductile region C

Fig. 8 shows transmission electron micrographs of HIP1 deformed at $\dot{\varepsilon} = 1 \times 10^{-4} s^{-1}$. The specimen in Fig. 8a and b was deformed to the maximum stress at 1673 K (region B). Many sharp cracks are seen along the grain boundaries, and few dislocations are present in most of the grains. The primary {1 1 0}⟨1 1 0⟩ slip and grain-boundary sliding cause stress concentration, but the insufficient number of independent slip systems cannot accommodate the stress concentration. This results in the formation of the sharp cracks and the consequent quasi-brittle fracture in region B.

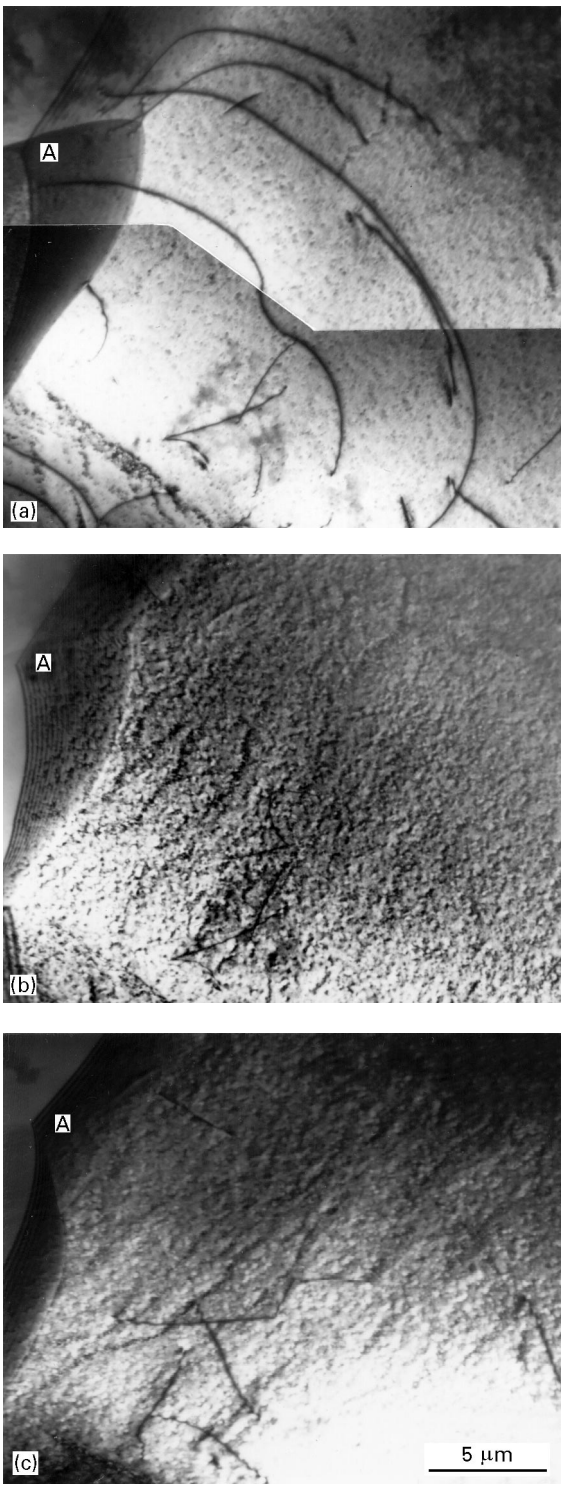

Figure 7 Dislocation substructure of HIP1 deformed at 1823 K (region C). Beam direction, $\boldsymbol{B}$, and diffraction condition, $\boldsymbol{g}$, are (a) $\boldsymbol{B} = [0\,1\,1]$ and $\boldsymbol{g} = \bar{1}\,\bar{1}\,1$, (b) $\boldsymbol{B} = [0\,1\,1]$ and $\boldsymbol{g} = \bar{2}\,0\,0$, and (c) $\boldsymbol{B} = [\bar{2}\,1\,1]$ and $\boldsymbol{g} = 1\,1\,1$. "A" indicates the same triple grain junction.

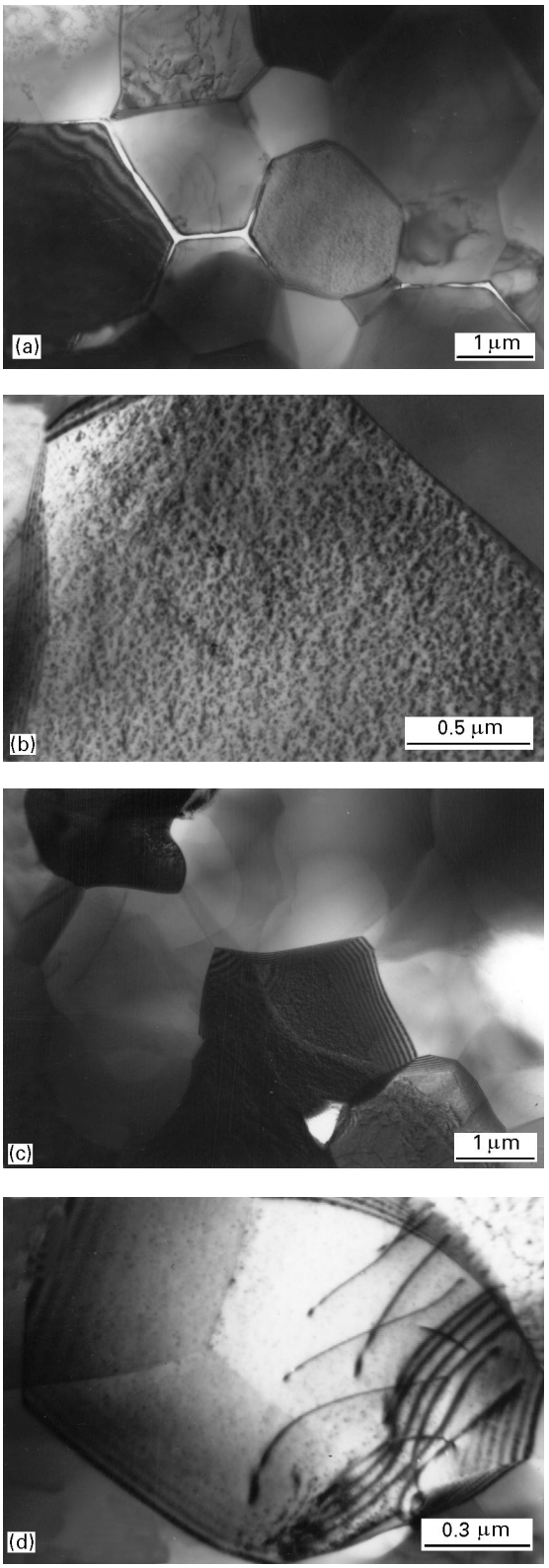

Figure 8 Microstructure of HIP1 deformed at $\dot{\varepsilon} = 1 \times 10^{-4}\,s^{-1}$. (a, b) Deformed at 1673 K (region B) to $\varepsilon = 0.03$; (c,d) tested at 1823 K (region C) to $\varepsilon = 0.18$.

The primary slip system of UO_2 $\{0\,0\,1\}\langle 1\,1\,0\rangle$ and Al_2O_3 $\{0\,0\,0\,1\}\langle 1\,1\,\bar{2}\,0\rangle$) cannot provide five independent slip systems [4]. In these materials, stress concentration due to the primary slip assists grain-boundary cracking in region B. Critical stress for the activation of the primary slip decreases with increasing temperature, resulting in a decrease of quasi-brittle fracture stress in UO_2 and Al_2O_3 [10, 11]. The decrease in quasi-brittle fracture stress of TiN can be explained by the same process.

The specimen in Fig. 8c and d was deformed to $\varepsilon = 0.18$ at 1823 K (region C). Dislocations are active in many grains. The sharp grain-boundary cracks in region B are replaced by round cavities at triple grain junctions. Five independent slip systems are available in this region. Stress concentration is readily released by plastic deformation as well as high diffusivity at the high temperature, resulting in the large ductility in region C. The activation of five independent slip systems is an important cause of the transition from quasi-brittle region B to ductile region C.

3.6. Deformation mechanism in region C

The slopes of $\log\sigma_M$ versus $1/T$ (Fig. 4) and $\log\sigma_M$ versus $\log\dot{\varepsilon}$ (Fig. 6) relations give the values of mQ and m in Equation 1, respectively. $mQ = 200\,kJ\,mol^{-1}$ and $m = 0.58$ in region C. The value of m close to 0.5 is typical of superplasticity [12]. From these values, one obtains $Q = 340\,kJ\,mol^{-1}$. A limited number of reports are available on the activation energy for diffusion of nitrogen in TiN. The reported values are in the range 152–377 $kJ\,mol^{-1}$ [13–16]. The value of Q determined experimentally is in this range, suggesting that plastic deformation in region C is controlled by diffusion of nitrogen ions.

Maximum stresses, σ_M, in region C are plotted against the initial grain sizes in Fig. 9. They decrease with decreasing grain size. The value of mp obtained from the slope of Fig. 9 is 0.77, and therefore the grain size exponent, p, is equal to 1.3. This result resembles the grain-boundary sliding model proposed by Langdon [17], predicting $m = 0.5$ and $p = 1$. However, p of Equation 1 has been reported to be 2–3 on superplasticity [12]. Grain growth took place during compression tests of HP0 ($d = 0.3\,\mu m$). The grain growth can reduce the apparent value of p. Superplastic deformation is primarily caused by grain-boundary sliding. An obvious increase in dislocation density,

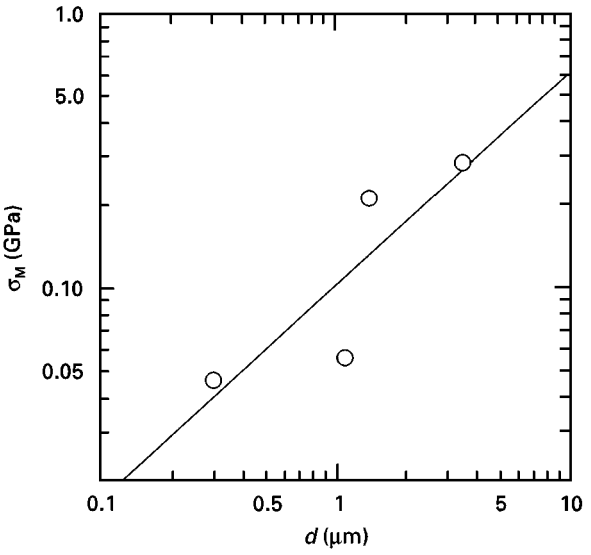

Figure 9 Effect of initial grain size, d, on maximum stress, σ_M, at $\dot{\varepsilon} = 1 \times 10^{-4}\,s^{-1}$ and 1823 K. The maximum stresses of HP0 and HP1 were obtained by extrapolation to 1823 K.

however, was observed in the TiN specimens [18], suggesting that dislocation creep ($p = 0$) also contributes to the superplastic deformation. The contribution of dislocation creep can be another cause of the deviation from $p = 2$–3.

4. Conclusions

1. The temperature dependence of maximum (fracture or peak) stress of TiN shows three regions with different activation energy and strain-rate sensitivity.
2. In the low-temperature region, brittle fracture takes place without plastic deformation. Fracture stress is independent of temperature, and greater than 1 Gpa. Maximum stress of TiN decreases, roughly speaking, above 1300 K.
3. In the intermediate temperature region, sharp cracks are formed along grain boundaries, because of the insufficient number of independent slip systems. Specimens fracture in a quasi-brittle manner after a few per cent plastic deformation. The fracture is assisted by the plastic deformation, and fracture stress is high at smaller grain size and lower porosity.
4. The appearance of a quasi-brittle regime is similar to MgO (ionic) but different from TiC (covalent). This fact suggests that the primary slip plane of TiN is $\{1\,1\,0\}$ (MgO type) rather than $\{1\,1\,1\}$ (TiC type). The Burgers vector of dislocations active in TiN is $1/2\langle 1\,1\,0\rangle$.
5. In the high-temperature region, five independent slip systems are available, so that TiN becomes ductile. Flow stress in this region decreases with decreasing grain size. Activation energy for plastic deformation is close to that for diffusion of nitrogen in TiN. Strain-rate sensitivity is typical of superplasticity.

Acknowledgements

The materials used were kindly provided by Nisshin Steel Co. Ltd. This research was supported by grants from JSPS (no. JSPS-RFTF96R12301) and from the Ministry of Education, Science, Sports and Culture, Japan (nos. 08455313 and 0824105).

References

1. R. L. FLEISCHER, *J. Metals* **37** Dec (1985) 16.
2. T. YAMADA, M. SHIMADA and M. KOIZUMI, *Am. Ceram. Soc. Bull.* **59** (1980) 611.
3. A. G. EVANS and T. G. LANGDON, *Prog. Mater. Sci.* **21** (1976) 171.
4. R. W. DAVIDGE, in "Mechanical Behaviour of Ceramics" (Cambridge University Press, Cambridge, 1979).
5. D. K. CHATTERJEE, M. G. MENDIRATTA and H. A. LIPSITT *J. Mater. Sci.* **14** (1979) 2151.
6. H. KURISHITA, K. NAKAJIMA and H. YOSHINAGA, *Mater Sci. Eng.* **54** (1984) 177.
7. D. B. MIRACLE and H. A. LIPSITT, *J. Am. Ceram. Soc.* **66** (1983) 592.
8. R. B. DAY and R. J. STOKES, *ibid.* **49** (1966) 345.
9. K. UEMATSU, M. NAKAMURA, Z. KATO, N. UCHIDA and K. SAITO, *J. Ceram. Soc. Jpn* **97** (1989) 63.
10. A. G. EVANS and R. W. DAVIDGE, *J. Nucl. Mater.* **33** (1969) 249.
11. H. MEREDITH and P. L. PRATT, in "Special Ceramics", edited by P. Popper (British Ceramic Research Association, Stoke-on-Trent, 1975) p. 107.
12. T. G. LANGDON, *Acta Metall. Mater.* **42** (1994) 2437.
13. R. J. WASILEWSKI and G. L. KEHL, *J. Inst. Metals* **83** (1954-55) 94.
14. V. S. EREMEEV, YU M. IVANOV and A. S. PANOV, *Izv. Akad. Nauk. SSSR Met.* **4** (1969) 262.
15. V. D. REPKIN, G. V. KURTUKOV, A. A. KORNILOV and V. V. BESPALOV, *Metalloterm. Protsessy Khim. Metall.* (1971) 320.
16. E. METIN and O. T. INAL, *Metall. Trans.* **20A** (1989) 1819.
17. T. G. LANGDON, *Philos. Mag.* **22** (1970) 689.
18. R. R. YAMAMOTO, K. MARUYAMA and H. OIKAWA, *Rept.* 123*rd Commun. JSPS* **36** (1995) 139.

Received 3 February
and accepted 5 December 1997